# Strain and x-ray diffraction from axial nanowire heterostructures

V. M. Kaganer
*Paul-Drude-Institut für Festkörperelektronik, Hausvogteiplatz 5–7, 10117 Berlin, Germany*

A. Yu. Belov
*Institute of Crystallography, Russian Academy of Sciences, 119333 Moscow, Russia*
(Received 15 December 2011; published 2 March 2012)

Lattice distortions in a cylindrical nanowire with nonuniform intrinsic strains arbitrarily varying along its axis are analyzed, with a special emphasis on heterostructures. We find that, as a result of the elastic relaxation on the side surface, the lateral mismatch does not change the average longitudinal lattice period of the whole cylinder, but effects the average period of heterostructure. As a consequence, the positions of the x-ray diffraction peaks due to a periodic axial heterostructure depend on the ratio of the total height of the whole heterostructure to the cylinder diameter. The peaks attain the positions of the planar heterostructure peaks only when the diameter becomes orders of magnitude larger than the heterostructure height. The typical nanowire heterostructure parameters correspond to the opposite limit of full lateral relaxation.

DOI: 10.1103/PhysRevB.85.125402 PACS number(s): 46.25.Cc, 61.05.cp, 61.46.Km, 68.65.Cd

## I. INTRODUCTION

Many applications of semiconductor nanowires in nanophotonic devices (in particular for photovoltaics and visible light emission) profit from the elastic strain relaxation due to the free side surface of the nanowires. The strain caused by the lattice mismatch in nanowire heterostructures releases more effectively compared to planar heterostructures.[1–3] However, the strain cannot release completely and a nonuniform three-dimensional distribution of strain remains in the nanowire.

X-ray diffraction is a primary tool to reveal strain in nanowires. The x-ray diffraction patterns are experimentally observed from heterostructures in nanowires prepared by different techniques: etching of the planar heterostructure,[4,5] vapor-liquid-solid mechanism,[6,7] and self-induced growth.[8–11] An appropriate strain analysis is required to obtain the structure parameters from these observations.

There are at least three different ways to evaluate strain distribution in nanowire heterostructures. The problem can be solved numerically in the framework of the continuum elasticity theory, using the finite element method.[4,6] An alternative numerical approach is atomistic and consists in minimization of a potential energy function, based on an interatomic potential properly reproducing elastic properties, for example, the Keating force field.[7–9] An obvious advantage of numerical methods is the possibility to consider arbitrary nanowire shapes.

For a circular cylinder of infinite length the elasticity problem can also be solved analytically. In general, the solution is sought as a sum of two terms: One is the known solution for a planar heterostructure and the other accounts for stress relaxation at the side surface of the cylinder. For the elastically isotropic cylinder with a layer undergoing uniform intrinsic strains, this latter term coincides with the solution for the cylinder with a part of the surface under external pressure[12] (see also Ref. 13, p. 388). This solution has been used to calculate the x-ray diffraction pattern from the nanowire heterostructure.[4] The corresponding extension of the result[12] to an anisotropic cylinder with transverse isotropy of the elastic constants (which includes, in particular, the hexagonal crystals) was given in Ref. 14 for a periodic array of layers and in Ref. 15 for a single layer.

X-ray diffraction is routinely used to determine the structure of planar heteroepitaxial layers and multilayers. The lattice mismatch determination from the diffraction peak positions is well established.[16–19] In particular the longitudinal (along the normal to the layers) shift of the diffraction peak is caused by both longitudinal and transverse mismatch. The peak shift due to the longitudinal mismatch is just a stress-free vertical expansion of the mismatched layer, while the peak shift due to the transverse mismatch is a Poisson effect. This result is also valid for a heterostructure in a cylinder of a sufficiently large diameter. In the opposite limit of a small cylinder diameter, each layer of the film freely expands laterally and the transverse mismatch does not cause a longitudinal expansion of the heterostructure.

We investigate the transition from one limit to the other, as the nanowire diameter is increased, and find that the transition depends not on the layer thickness but on the height of the whole heteroepitaxial structure. In other words, when the heterostructure period remains the same, the transition in the diffraction pattern from the one of a free lateral expansion of each layer to the planar heterostructure case depends on the number of periods in the heterostructure. It starts when the nanowire diameter exceeds the height of the whole heterostructure and reaches the planar heterostructure limit at about two orders of magnitude larger diameters.

We show that this behavior is a consequence of a quite general property of the strain due to a mismatched layer in a cylinder. Namely, the transverse mismatch gives rise, due to stress relaxation at the side cylinder surface, to an additional strain that decays along the cylinder on the distances comparable with diameter. As a result, when only the transverse mismatch is considered, the relative displacement of the cylinder well above and well below the layer is identically zero.

The x-ray diffraction peak positions from a heterostructure correspond to the mean strain in it rather than in the entire

 ©2012 American Physical Society

nanowire. As long as the heterostructure height is larger than the nanowire diameter, the relaxation described above proceeds inside the heterostructure. Due to this relaxation, diffraction peaks are at the same positions as in the case of a free lateral expansion of each layer, despite the layers being strained. The practical nanowire diameters and heterostructure thicknesses correspond to this limit. When the height of the whole layer stack becomes smaller than the diameter, the relaxation only partially takes place inside the heterostructure and the transverse mismatch provides some additional shift of diffraction peaks. The limit of a planar heterostructures is reached at much larger diameters.

## II. ELASTICITY OF A CYLINDRICAL NANOWIRE WITH INTRINSIC STRAINS

### A. Plane-stress solution for an embedded layer

Let us consider first a mismatched layer embedded in a laterally infinite matrix, which is also assumed to be of infinite thickness. The solution of this problem is well known and is a basis for the x-ray diffraction analysis of the planar heterostructures.[16–19] We use it as a reference in further analysis of the corresponding elastic problem in a cylinder. Hence the solution is given in cylindrical coordinates. We also discuss its accuracy and limitations, paying attention to the assumptions made in the derivation.

The strains can be found for a general case of a continuous variation of the longitudinal $c(z)$ and the lateral $a(z)$ lattice parameters in the layer, where $z$ is the coordinate along its normal. Throughout the paper both the matrix and the layer are assumed to possess the hexagonal crystal lattice with the sixfold axis in the $z$ direction. Hence the system possesses the transverse elastic isotropy. The relative difference of the layer lattice parameters with respect to the matrix is characterized by the strains $e^*_\perp(z) = a(z)/a_0 - 1$ and $e^*_\parallel(z) = c(z)/c_0 - 1$, where $a_0$ and $c_0$ are the respective lattice parameters of the matrix. If a layer with the constant strains $e^*_\perp(z) = e^0_\perp$ and $e^*_\parallel(z) = e^0_\parallel$ is detached from the matrix and becomes free of stress, the strains in it are the intrinsic strains $e^*_{rr} = e^*_{\theta\theta} = e^0_\perp$ and $e^*_{zz} = e^0_\parallel$, where cylindrical coordinates are used. This strain (also called self-strain, eigenstrain, or transformation strain) itself does not cause stress. The stress arises due to the requirement of coherency for the crystal lattices of the layer and the matrix, which is referred to as the strain compatibility condition. If the coherency is lost by formation of misfit dislocations, the above expressions for the intrinsic strains must be modified by taking into account the plastic strain associated with misfit dislocations.

It is worth noting that, in general, the nonuniform transverse intrinsic strain $e^*_\perp(z)$ is not compatible and induces stress in the layer, even if the compatibility condition at the matrix-layer interface is fulfilled. The only exception is the strain varying linearly with $z$: $e^*_\perp(z) = e^*_\perp(0) + Cz$, where $C$ is a constant. In this particular case the stress does not occur upon the layer detachment from the matrix. In turn, the one-dimensional longitudinal intrinsic strain $e^*_\parallel(z)$ is compatible and does not cause stress for any dependence on $z$. For the analysis of the diffraction pattern, one has to take into account that the change of the lattice spacings is described by the total strain $\hat{\varepsilon}$, which is the sum of the intrinsic strain and the elastic strain $\hat{e}$, $\hat{\varepsilon} = \hat{e}^* + \hat{e}$. The latter is due to bond stretching and is related to the stress $\hat{\sigma}$ by Hooke's law.

Two boundary conditions determine strain in a planar matrix-layer system. First, the layer can freely expand along its normal and hence the stress in the vertical direction is absent, $\sigma_{zz} = 0$, in the entire system, resulting in the plane-stress state. Second, the matrix does not allow a lateral expansion of the layer. Then the lateral components of the total strain are absent, $\varepsilon_{rr} = \varepsilon_{\theta\theta} = 0$. In addition, one has $\sigma_{rr} = \sigma_{\theta\theta}$ due to isotropy of the intrinsic strains and the elastic constants in the lateral plane. This approximation is commonly used for strain analysis in planar heterostructures on an infinite substrate. It is valid only for sufficiently thick systems and fails when the thickness of the matrix becomes comparable with that of the layer. The present analysis is restricted with a sufficiently thick matrix.

The relations between stress and strain components for hexagonal symmetry are collected in the Appendix. Using Hooke's law (A2), the condition $\sigma_{zz} = 0$ can be written as

$$2c_{13}(\varepsilon_{rr} - e^*_\perp) + c_{33}(\varepsilon_{zz} - e^*_\parallel) = 0. \tag{1}$$

Since $\varepsilon_{rr} = 0$, the longitudinal total strain in the layer $\varepsilon_{zz}$ can be calculated as

$$\varepsilon_{zz} = e^*_\parallel + \frac{2c_{13}}{c_{33}} e^*_\perp. \tag{2}$$

Let us consider a more general case of a diffuse interface between the matrix and the layer and introduce a dimensionless profile, or shape, function $g(z)$, describing the variation of the intrinsic strain in the interface and characterizing its width. The shape function is assumed to be symmetric, $g(-z) = g(z)$. The origin $z = 0$ is chosen in the middle plane of the layer. Then one can represent the intrinsic strain components as

$$e^*_\perp(z) = e^0_\perp g(z), \quad e^*_\parallel(z) = e^0_\parallel g(z), \tag{3}$$

where $e^0_\perp$ and $e^0_\parallel$ are constants and $g(z) \to 0$ as $|z| \to \infty$. Equal strains $e^0_\perp = e^0_\parallel$ are frequently taken in the numerical calculations, but it is advantageous to distinguish these components in the analysis because they provide qualitatively different contributions to the strain fields.

The normal displacement $u^0_z(z)$ can be obtained by the total strain integration

$$u^0_z(z) = \left(e^0_\parallel + \frac{2c_{13}}{c_{33}} e^0_\perp\right) \int_0^z g(z)dz. \tag{4}$$

Particularly for a uniform layer with thickness $2d$ and sharp interfaces, we obtain

$$\begin{aligned} u^0_z(z) &= \left(\frac{2c_{13}}{c_{33}} e^0_\perp + e^0_\parallel\right) z \quad \text{for} \quad |z| \leqslant d, \\ u^0_z(z) &= \left(\frac{2c_{13}}{c_{33}} e^0_\perp + e^0_\parallel\right) d\,\mathrm{sgn}(z) \quad \text{for} \quad |z| > d. \end{aligned} \tag{5}$$

The stress in the layer can be found by using Hooke's law (A1),

$$\varepsilon_{rr} = \varepsilon_{\theta\theta} = e^*_\perp + (s_{11} + s_{12})\sigma^0_{rr} = 0, \tag{6}$$

and therefore

$$\sigma^0_{rr} = \sigma^0_{\theta\theta} = -\frac{e^*_\perp}{s_{11} + s_{12}} = -\sigma^0 g(z), \quad \sigma^0_{zz} = 0, \tag{7}$$

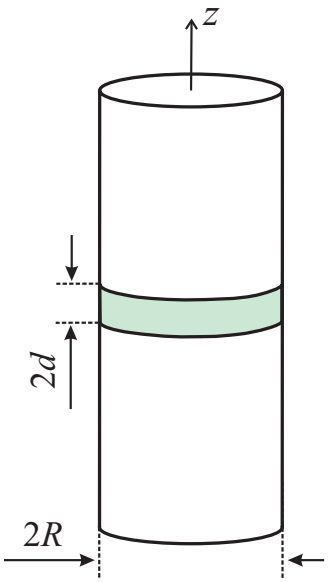


FIG. 1. (Color online) Geometry of a mismatched layer with sharp interfaces in cylindrical nanowire.

where it is defined

$$\sigma^0 = \left(c_{11} + c_{12} - \frac{2c_{13}^2}{c_{33}}\right)e_\perp^0. \tag{8}$$

### B. Exact solution for a layer in the cylinder

Consider a cylindrical nanowire of diameter $2R$ with a one-dimensional distribution of intrinsic strains given by Eq. (3). Formulas below are derived for an arbitrary $z$-dependent distribution of the intrinsic strains, continuous or discontinuous. We do not restrict ourselves to the particular case of a uniform mismatched layer of thickness $2d$, as drawn in Fig. 1.

The solution of the elastic problem for a planar layer obtained above gives nonzero stress on the side cylinder surface. The solution of the elastic problem for the cylinder is sought as a sum of two terms: the strain field produced by the intrinsic strain $e_{kl}^*(z)$ in an infinite medium calculated above and the image strain field required to satisfy the boundary conditions on the side surface of the cylinder $r = R$,

$$\sigma_{rr}(R,z) = 0, \quad \sigma_{rz}(R,z) = 0. \tag{9}$$

The stress components are the sums

$$\sigma_{ij}(r,z) = \sigma_{ij}^0(z) + \sigma_{ij}^{\rm im}(r,z), \tag{10}$$

where the stresses $\sigma_{ij}^0(z)$ are given by Eq. (7). The displacements $u_i(r,z)$ in the cylinder are represented similarly as sums

$$u_i(r,z) = u_i^0(z) + u_i^{\rm im}(r,z), \tag{11}$$

where $u_z^0(z)$ is given by Eq. (4) and the other components $u_r^0$ and $u_\theta^0$ are zero.

The boundary value problem for the image field is solved by representing the shape function $g(z)$ by its Fourier spectrum $g(q)$,

$$g(z) = \int_0^\infty g(q)\cos(qz/R)dq. \tag{12}$$

The solution is obtained for each Fourier component, using the axially symmetric stress functions[20,21] to represent the displacement field. The solution is given in the Appendix. Using dimensionless coordinates

$$x = r/R, \quad \zeta = z/R, \tag{13}$$

the image displacements are written as

$$u_r^{\rm im}(x,\zeta) = -\frac{R\sigma^0}{c_{44}}\int_0^\infty \left[\frac{1}{1+k_1}\frac{I_1(qx/\nu_1)}{I_1(q/\nu_1)} - \frac{1}{1+k_2}\frac{I_1(qx/\nu_2)}{I_1(q/\nu_2)}\right] \times \frac{g(q)}{D(q)}\cos q\zeta\, dq, \tag{14}$$

$$u_z^{\rm im}(x,\zeta) = \frac{R\sigma^0}{c_{44}}\int_0^\infty \left[\frac{k_1\nu_1}{1+k_1}\frac{I_0(qx/\nu_1)}{I_1(q/\nu_1)} - \frac{k_2\nu_2}{1+k_2}\frac{I_0(qx/\nu_2)}{I_1(q/\nu_2)}\right] \times \frac{g(q)}{D(q)}\sin q\zeta\, dq. \tag{15}$$

Here $I_0(x)$ and $I_1(x)$ are modified Bessel functions and

$$D(q) = \frac{c_{11}-c_{12}}{c_{44}}\frac{k_2-k_1}{(1+k_1)(1+k_2)} - q\left(\nu_1\frac{I_0(q/\nu_1)}{I_1(q/\nu_1)} - \nu_2\frac{I_0(q/\nu_2)}{I_1(q/\nu_2)}\right). \tag{16}$$

The parameters $\nu_1$, $\nu_2$, $k_1$, and $k_2$ are defined in the Appendix.

For the layer with a constant intrinsic strain and sharp interfaces shown in Fig. 1, $g(z)$ reduces to the step function represented by the Fourier integral

$$g(z) = [\mathrm{sgn}(z+d) - \mathrm{sgn}(z-d)]/2 = \frac{2}{\pi}\int_0^\infty \frac{\sin(qd/R)}{q}\cos(qz/R)dq. \tag{17}$$

Hence its spectrum is

$$g(q) = \frac{2}{\pi}\frac{\sin(qd/R)}{q}. \tag{18}$$

In this case, Eqs. (14) and (15) are equivalent to the results of Ref. 15 represented by means of an alternative stress function. Strain is obtained by differentiation of the displacements (14) and (15). Explicit expressions for strain components are given in the Appendix.

Let us now consider the asymptotic behavior of the image displacements at $\zeta \gg 1$. Taking into account the behavior of cylindrical functions at small $q$, one can show that at $\zeta \gg 1$ the longitudinal displacement is represented as

$$u_z^{\rm im}(x,\zeta) = \frac{R\sigma^0}{c_{44}}\frac{2}{D(0)}\left[\frac{k_1\nu_1^2}{1+k_1} - \frac{k_2\nu_2^2}{1+k_2}\right] \times \int_0^\infty g(q)\frac{\sin q\zeta}{q}dq. \tag{19}$$

For further analysis of Eq. (19), we proceed to the real-space integral of the shape function,

$$\int_0^\infty g(q)\frac{\sin q\zeta}{q}dq = R^{-1}\int_0^z g(z)dz. \tag{20}$$

Then, at $\zeta \gg 1$,

$$u_z^{\rm im}(x,\zeta) = \frac{\sigma^0}{c_{44}}\frac{2}{D(0)}\left[\frac{k_1\nu_1^2}{1+k_1} - \frac{k_2\nu_2^2}{1+k_2}\right]\int_0^z g(z)dz. \quad (21)$$

Correspondingly, the displacement in the cylinder in the limit $z \to \infty$ is

$$u_z(x,\zeta \to \infty) = (Ae_\perp^0 + e_\parallel^0)\int_0^\infty g(z)dz, \quad (22)$$

where

$$A = \frac{2\left(c_{11}+c_{12}-2c_{13}^2/c_{33}\right)}{c_{44}D(0)}\left[\frac{k_1\nu_1^2}{1+k_1} - \frac{k_2\nu_2^2}{1+k_2}\right] + \frac{2c_{13}}{c_{33}}. \quad (23)$$

A direct calculation of the coefficient $A$ in Eq. (23) shows that $A = 0$ and therefore the relative displacement of the cylinder ends $\Delta L = u_z(r,\infty) - u_z(r,-\infty)$ depends only on the average longitudinal intrinsic strain

$$\Delta L = \int_{-\infty}^{\infty} e_\parallel^*(z)dz. \quad (24)$$

Hence the lateral mismatch $e_\perp^0$ does not change the average longitudinal lattice spacing. This result contrasts with the prediction based on the conventional solution, given in Eq. (4) or (5), which ignores the stress relaxation at the side surface of the cylinder. This result, as we show in Sec. III, essentially effects the x-ray diffraction peak positions for nanowire heterostructures. Equation (24), derived here from the exact solution of the corresponding anisotropic elasticity problem, has a clear physical origin and can be explained within the framework of the average stress theorem[22] for finite elastic bodies with inhomogeneous intrinsic strains and a traction-free surface.

### C. Solution for planar heterostructures in free-standing films

In the analysis of embedded planar heterostructures in Sec. II A, the stress boundary condition on the side surface due to the elastic strain in the layer was ignored. In the case of free-standing films we can take it into account approximately by replacing the exact condition of stress relaxation with the requirement of the corresponding average stress vanishing.

For a planar free-standing film of thickness $L$ with a one-dimensional distribution of intrinsic strains $e_{kl}^*(z)$ the stresses $\sigma_{iz}$ vanish and the nonzero components of the stress tensor are given by[22]

$$\sigma_{ij}(z) = -c_{ijkl}^*(\mathbf{n})[e_{kl}^*(z) - \overline{e_{kl}^*}], \quad (25)$$

where

$$\overline{e_{kl}^*} = \frac{1}{L}\int_{-L/2}^{L/2} e_{kl}^*(z)dz \quad (26)$$

is the average intrinsic strain in the film, $\mathbf{n}$ is a unit vector along $z$ axis, and the planar tensor of elastic constants for the direction $\mathbf{n}$ is given by

$$c_{ijkl}^*(\mathbf{n}) = c_{ijkl} - c_{ijmp}n_m(nn)_{pq}^{-1}n_r c_{rqkl}. \quad (27)$$

Here $(nn)_{pq} = n_i c_{ipqj} n_j$ and the tensor $(nn)^{-1}$ is the inverse to the tensor $(nn)$. The relation (25) between stresses and intrinsic strains in the film is derived under the assumption that $e_{kl}^*(-z) = e_{kl}^*(z)$ to exclude the film bending effects. Equation (25) ensures that the average stress in the film vanishes and therefore the boundary conditions for the stress at the side surface ($r = R,z$) are satisfied approximately, in the form $\overline{\sigma}_{rr} = \overline{\sigma}_{r\theta} = \overline{\sigma}_{rz} = 0$.

For hexagonal crystal symmetry and a transversely isotropic tensor of intrinsic strains with the components $e_{rr}^*(z) = e_{\theta\theta}^*(z) = e_\perp^*(z)$ and $e_{zz}^*(z) = e_\parallel^*(z)$, the nonzero stress components given by Eq. (25) reduce to

$$\sigma_{rr} = \sigma_{\theta\theta} = -\left(c_{11}+c_{12}-\frac{2c_{13}^2}{c_{33}}\right)[e_\perp^*(z) - \overline{e_\perp^*}]. \quad (28)$$

Using Hooke's law, the in-plane elastic strain related to the stress (28) can be written as

$$e_{rr} = e_{\theta\theta} = -[e_\perp^*(z) - \overline{e_\perp^*}]. \quad (29)$$

Since the film has the freedom to expand in the $z$ direction, the normal elastic strain can be calculated from the condition $\sigma_{zz} = 0$ as

$$e_{zz} = \frac{2c_{13}}{c_{33}}[e_\perp^*(z) - \overline{e_\perp^*}]. \quad (30)$$

The total strain $\varepsilon_{kl}(z)$ is the sum of the intrinsic strain $e_{kl}^*(z)$ and the elastic strain $e_{kl}(z)$. Since the lateral expansion of the film is controlled by the compatibility condition, the in-plane components of the total strain remain constant

$$\varepsilon_{rr} = \varepsilon_{\theta\theta} = \overline{e_\perp^*}. \quad (31)$$

However, in contrast to Sec. II A, they vanish only as the average intrinsic strain $\overline{e_\perp^*}$ vanishes. In turn, the total strain $\varepsilon_{zz}$ can now be calculated as

$$\varepsilon_{zz} = e_\parallel^*(z) + \frac{2c_{13}}{c_{33}}[e_\perp^*(z) - \overline{e_\perp^*}]. \quad (32)$$

The corresponding displacements $u_i$ become

$$\begin{aligned} u_r(r) &= \overline{e_\perp^*}r, \\ u_z(z) &= \int_0^z \left\{e_\parallel^*(z) + \frac{2c_{13}}{c_{33}}[e_\perp^*(z) - \overline{e_\perp^*}]\right\}dz. \end{aligned} \quad (33)$$

It follows from Eq. (33) that the change in the film thickness $\Delta L = u_z(r,L/2) - u_z(r,-L/2)$ is independent of the stress distribution in it and results only from the average longitudinal intrinsic strain

$$\Delta L = \int_{-L/2}^{L/2} e_\parallel^*(z)dz, \quad (34)$$

in accordance with Eq. (24).

For a layer of thickness $2d$ with the uniform intrinsic strain and sharp interfaces, we have $\overline{e_\perp^*} = (2d/L)e_\perp^0$. The total strain $\varepsilon_{zz}$ inside the layer ($|z| < d$) can now be calculated as

$$\varepsilon_{zz} = e_\parallel^0 + \frac{2c_{13}}{c_{33}}e_\perp^0\left(1 - \frac{2d}{L}\right), \quad (35)$$

whereas the stress components become

$$\sigma_{rr} = \sigma_{\theta\theta} = -\sigma^0[1 - (2d/L)], \quad \sigma_{zz} = 0. \quad (36)$$

The longitudinal displacement $u_z$ is

$$u_z(z) = u_z^0(z) - \frac{2d}{L}\frac{2c_{13}}{c_{33}}e_\perp^0 z, \tag{37}$$

where $u_z^0(z)$ is given by Eq. (5). Equations (35)–(37) enable us to estimate the accuracy of the results obtained in Sec. II A in the limit $L \gg d$. Thus one can see that the second term in Eq. (37) can be neglected when the displacement is calculated in the vicinity of the layer, $z/d \sim 1$, and the equations of Sec. II A can be used. However, the terms of the order of $d/L$ cannot be neglected when the displacement is calculated at distances $z \approx L$, particularly in the calculation of the change in the thickness of the whole system $\Delta L = 2e_\parallel^0 d$.

### D. Displacement distributions

We use the formulas derived above to calculate the distributions of the displacements. Figure 2 shows the $z$ component of the displacements. The ratio of the disk height $2d$ to the disk diameter $2R$ is taken to be $d/R = 0.1$. We set $\varepsilon_\parallel^0 = \varepsilon_\perp^0 = \varepsilon^0$ and scale the displacements by $R\varepsilon^0$. The displacement in the infinite medium (5) is shown in Fig. 2(a). It is just the linear function inside the layer.

The image displacement (15) is shown in Fig. 2(b). Near the surface, the displacement $u_z^{\rm im}$ inverts the sign. The longitudinal displacement caused by only transverse lattice mismatch ($\varepsilon_\parallel^0 = 0, \varepsilon_\perp^0 \neq 0$) is of special interest. It is denoted by $u_z^\perp(r,z)$ and is shown in Fig. 2(c): The displacement tends to zero for $|z| \gg R$, as found in the preceding sections. We recall that the stress-free boundary conditions are applied at the ends of cylinder and the cylinder is free to extend along its axis. However, the displacement occurs localized in the region with the height comparable with the cylinder diameter. The displacements $u_z(r,z)$ given by Eq. (11) are shown in Fig. 2(d).

The radial displacement is presented in Fig. 3. The displacement $u_r(r,z)$ coincides with the image displacement $u_r^{\rm im}(r,z)$. The radial displacement is zero at the cylinder axis,

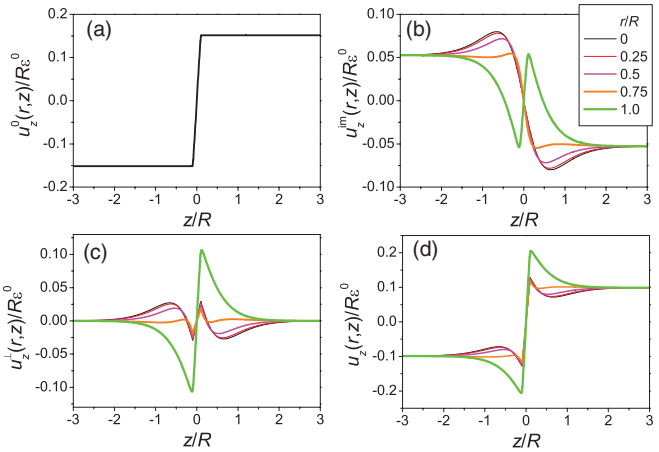


FIG. 2. (Color online) Components of the longitudinal displacement $u_z$: (a) displacement in a planar film, (b) an additional contribution due to the boundary conditions in cylinder, (c) displacements due to the in-plane mismatch $\epsilon_\perp^0$, and (d) the complete displacement.

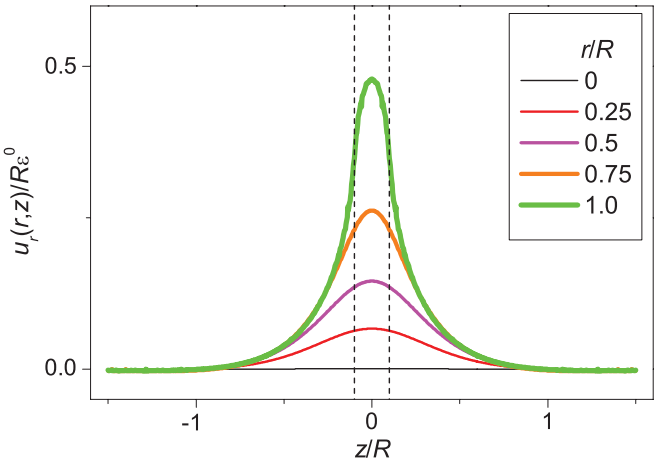


FIG. 3. (Color online) Radial displacement $u_r$ for a mismatched layer in the cylinder. Dashed lines show the layer borders.

as it follows from the symmetry of the problem, and increases toward the surface. The vertical dashed lines denote the layer borders. The displacements extend to a distance comparable with the cylinder radius $R$ rather than the layer thickness $d$.

## III. X-RAY DIFFRACTION FROM NANOWIRE HETEROSTRUCTURES

X-ray diffraction is a standard tool used to determine the structure of planar heteroepitaxial films and x-ray diffraction patterns are well understood.[16–19] Periodic layers give rise to satellite reflections. The distance between satellites directly provides the period of the heterostructure and the position of the zeroth-order reflection gives the average mismatch in the heterostructure. The x-ray diffraction from a nanowire heterostructure suffers from the inhomogeneous strain distribution in the nanowire. In comparison with the planar heterostructures, one more parameter, the ratio of the heterostructure height to the nanowire diameter, comes into consideration. In the limit of a very large diameter, the strain state of the heterostructure tends to that of a planar heterostructure. The thinner the nanowire, the better strain relaxation is on the side surface, which influences x-ray diffraction peaks.

X-ray diffraction is sensitive to the total displacements of atoms with respect to their positions in a reference crystal, the base of the nanowire. These displacements $u_i(r,z)$ are given by Eq. (11). The longitudinal displacement $u_z$ is the sum of two contributions, the displacement $u_z^0(z)$ for a planar film (5) and the image displacement $u_z^{\rm im}(r,z)$ given by Eq. (15), which provides stress relaxation on the side cylinder surface. The displacement due to a set of such disks is just the sum of the displacements from individual disks due to linear elasticity.

Figure 4(a) presents the longitudinal displacements $u_z(r,z)$ for a periodic structure with five layers. They model (In,Ga)N quantum wells in GaN nanowires. The well thickness is 6 nm, the spacing between the wells is 14 nm, and the nanowire diameter is 100 nm. Two curves show the displacement along the nanowire axis ($r = 0$) and along its surface ($r = R$). A corresponding planar heterostructure would possess an $r$-independent linear increase of the displacement $u_z^0(z)$

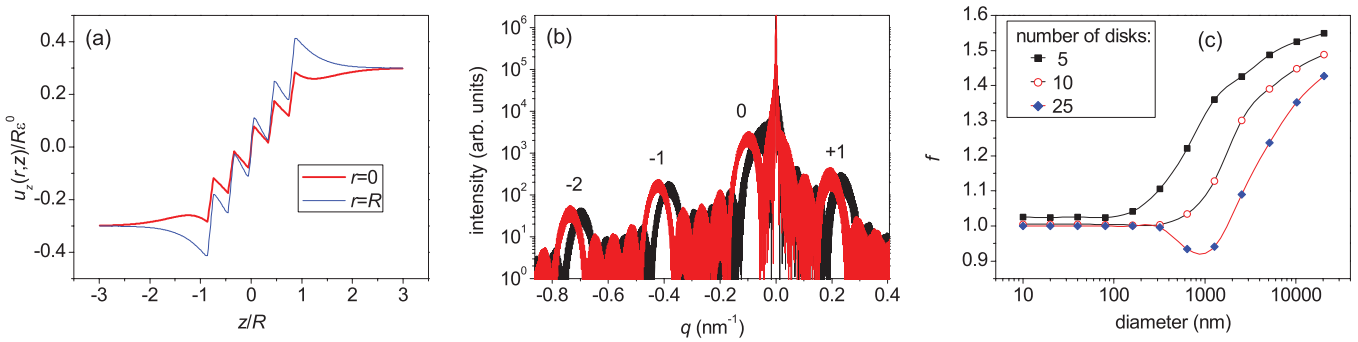


FIG. 4. (Color online) (a) Displacements $u_z(r,z)$ along the nanowire axis [$r = 0$, thick (red) line] and at the nanowire surface [$r = R$, thin (blue) line] for a periodic sequence of five mismatched layers. The disk thickness is 6 nm, the distance between disks is 14 nm, and the nanowire diameter is 100 nm. (b) Calculated x-ray diffraction pattern for a periodic sequence of ten such disks [thick (black) line] and diffraction pattern for a planar heterostructure with the same parameters [thin (red) line]. (c) Nanowire diameter dependence of the relaxation factor $f$ [Eq. (39)].

inside the wells with horizontal plateaus in the spacing layers between the wells. The difference in displacements causes the difference between diffraction patterns of the nanowire and the planar heterostructure.

Figure 4(b) shows the x-ray diffraction pattern calculated as

$$I(q) = \left| \int_{-\infty}^{\infty} \int_{0}^{R} \exp[i\,Q_0 u_z(r,z) + iqz] r\,dr\,dz \right|^2. \quad (38)$$

Here a longitudinal scan in symmetric Bragg reflection is considered, so only the $z$ displacement is of interest. The reciprocal lattice vector $Q_0$ is taken for the GaN(0002) reflection, $Q_0 = 24.1$ nm$^{-1}$. We take ten periodic quantum wells with the same parameters as above to have sharper diffraction peaks. The integral (38) is taken over the volume of the nanowire. Practical calculations are performed in a finite $z$ range, which causes artificial high-frequency fringes due to sharp ends of the nanowire. They can be smoothed by an appropriate resolution function.

The calculation for a nanowire heterostructure [thick black line in Fig. 4(b)] is compared with the calculation for a planar heterostructure with the same parameters (thin red line). Both curves show the same intensities of the satellite reflections and the same distances between reflections, but the reflections are shifted with respect to each other. The shift $\Delta q_0$ of the zeroth-order diffraction peak of the heterostructure with respect to the reference peak of the substrate (for a planar heterostructure) or the base (for a nanowire) can be written as

$$\Delta q_0/Q_0 = (2d/p) f \varepsilon^0. \quad (39)$$

In the x-ray diffraction calculations, we take equal values of misfits in the basal plane $\varepsilon^0_\perp = \Delta a/a$ and along the nanowire axis $\varepsilon^0_\parallel = \Delta c/c$. The thickness of the mismatched layers is $2d$ and the period of the heterostructure is denoted by $p$. The ratio $2d/p$ is the fraction of the period occupied by the layer and $(2d/p)\,\varepsilon^0$ is the average misfit.

The factor $f$ describes relaxation of the heterostructure. For planar films, the relaxation factor is given by Eq. (5),

$$f_{\text{planar}} = 2c_{13}/c_{33} + 1. \quad (40)$$

For the elastic moduli of GaN given in the Appendix, one has $f_{\text{GaN}} = 1.53$. In the limit of elastic isotropy, this factor becomes $f_{\text{planar}} = (1+\nu)/(1-\nu)$, where $\nu$ is the Poisson ratio.

In the opposite limit of the nanowire diameter small compared to the mismatched layer thickness, the layer is free to relax laterally, which gives $f = 1$. The layer in a nanowire relaxes partially, depending on the ratio of its thickness to the nanowire diameter, and the relaxation factor varies between 1 and $f_{\text{planar}}$. This range of relaxation factors has been already discussed[11] in the x-ray diffraction analysis of the (In,Ga)N/GaN nanowire heterostructures.

Using the solution of the elastic problem for a mismatched layer, we are able now to determine the dependence of the factor $f$ on the nanowire diameter. We have calculated the x-ray diffraction patterns, similar to the one in Fig. 4(b), for the same heterostructure period described above, but different numbers of periods and different nanowire diameters. The relaxation parameter $f$ obtained from the diffraction peak positions calculated by Eq. (39) is plotted in Fig. 4(c). We have used the first positive and negative reflection orders to obtain $f$. For the 25-period heterostructure, the use of the zeroth-order satellite gives the same result. For shorter superlattices and with $\varepsilon^0 = 0.01$ used in the calculations, there are deviations caused by the interference of the heterostructure signal with that of the nanowire base. When the misfit $\varepsilon^0$ is increased and the peaks become well separated, the use of the zeroth or first positive and negative orders gives the same result.

The transition from $f = 1$ for small cylinder diameters to $f = f_{\text{planar}}$ for very large cylinder diameters is clearly seen for all heterostructures. However, the diameters where this transition takes place depend on the number of heterostructure periods or, equivalently, on the total thickness of the whole heterostructure. The deviation from $f = 1$ begins when the diameter exceeds the heterostructure thickness and reaches $f_{\text{planar}}$ at diameters about two orders of magnitude larger.

The features of the strain field caused by a mismatched layer, described in Sec. II, explain this behavior. The longitudinal displacement caused by the transverse mismatch tends to zero for distances exceeding the cylinder diameter

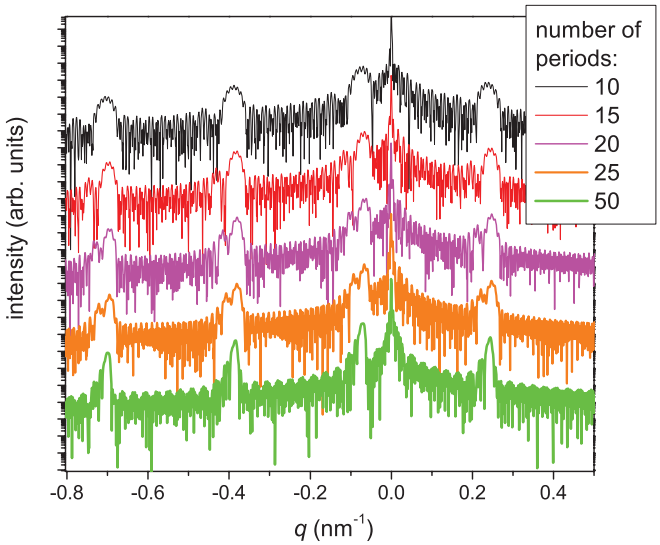


FIG. 5. (Color online) Transformation of the diffraction pattern with increasing number of periods in the heterostructure. The cylinder diameter is 700 nm.

[see Fig. 2(c)]. Diffraction peaks of a periodic heterostructure reveal the mean strain in the region occupied by the heterostructure. As long as its thickness exceeds the diameter, the strain is averaged over the whole essential region. As a result, the transverse mismatch does not contribute to the peak shift and $f$ remains close to 1. With a further increase of diameter, only part of the image strain field occurs inside the heterostructure and the effect of the side surface relaxation decreases. The factor $f$ continuously increases and at very large diameters reaches the limit of a planar heterostructure.

The factor $f$ for the 25-period heterostructure shows a minimum $f < 1$ for diameters comparable with the heterostructure height [see Fig. 4(c)]. This minimum is not simply a shift of diffraction peaks but a result of a more complicated transformation of the diffraction pattern, as shown in Fig. 5. Here the heterostructure period was kept the same as above ($p = 20$ nm) and the diameter was taken to be constant $2R = 700$ nm. As the number of periods in the heterostructure is increased, the shape of the diffraction peaks becomes more complicated. This is caused by nonuniformity of the image displacement: Different heterostructure parts occur under different strain conditions. The diffraction peak position and width do not completely characterize the diffraction pattern in this case.

## IV. CONCLUSION

The lateral mismatch in a heteroepitaxial film causes, as the Poisson effect, longitudinal strain and longitudinal film expansion. We show that, as a result of the elastic relaxation at the side surface of the cylinder, a long cylinder containing a layer with the lateral mismatch does not change the length, so the average longitudinal strain is zero. Since the relaxation occurs at distances comparable with the cylinder diameter, the x-ray diffraction peak positions from the axial heterostructures depend on the length of the whole heterostructure. As long as the heterostructure is shorter than the diameter, the peak position corresponds to full lateral relaxation of each layer. The practical nanowire heterostructures correspond to this limit. The opposite limit of a planar heterostructure is reached at two orders of magnitude larger diameters. These results provide a firm background for the x-ray diffraction analysis of nanowire heterostructures.

## ACKNOWLEDGMENTS

V.M.K. thanks Oliver Brandt and Martin Wölz for stimulating discussions.

## APPENDIX: ELASTIC CYLINDER WITH INHOMOGENEOUS INTRINSIC STRAINS

For a crystal with a hexagonal lattice (for example, GaN with the point group $6mm$) and the sixfold axis in the $z$ direction, Hooke's law in a cylindrical coordinate system $(r,\theta,z)$ retains the same form as it has in Cartesian coordinates:

$$\begin{aligned} e_{rr} &= s_{11}\sigma_{rr} + s_{12}\sigma_{\theta\theta} + s_{13}\sigma_{zz}, \\ e_{\theta\theta} &= s_{12}\sigma_{rr} + s_{11}\sigma_{\theta\theta} + s_{13}\sigma_{zz}, \\ e_{zz} &= s_{13}(\sigma_{rr} + \sigma_{\theta\theta}) + s_{33}\sigma_{zz}, \\ 2e_{\theta z} &= s_{44}\sigma_{\theta z}, \quad 2e_{rz} = s_{44}\sigma_{rz}, \quad 2e_{r\theta} = s_{66}\sigma_{r\theta} \end{aligned} \tag{A1}$$

and

$$\begin{aligned} \sigma_{rr} &= c_{11}e_{rr} + c_{12}e_{\theta\theta} + c_{13}e_{zz}, \\ \sigma_{\theta\theta} &= c_{12}e_{rr} + c_{11}e_{\theta\theta} + c_{13}e_{zz}, \\ \sigma_{zz} &= c_{13}(e_{rr} + e_{\theta\theta}) + c_{33}e_{zz}, \\ \sigma_{\theta z} &= 2c_{44}e_{\theta z}, \quad \sigma_{rz} = 2c_{44}e_{rz}, \quad \sigma_{r\theta} = 2c_{66}e_{r\theta}. \end{aligned} \tag{A2}$$

One has, in addition, $2c_{66} = c_{11} - c_{12}$ and $s_{66} = 2(s_{11} - s_{12})$. We use the following values for the elastic constants of wurtzite GaN at room temperature (in GPa):[23] $c_{11} = 390$, $c_{12} = 145$, $c_{13} = 106$, $c_{33} = 398$, and $c_{44} = 105$.

According to Ref. 21, for hexagonal crystals with axially symmetric strain distributions the image fields necessary to obey the boundary conditions can be derived from two quasiharmonic stress functions[20] $\phi_1(x,\zeta)$ and $\phi_2(x,\zeta)$ satisfying the following equations:

$$\left[\frac{\partial^2}{\partial x^2} + \frac{1}{x}\frac{\partial}{\partial x} + \frac{1}{\nu_j^2}\frac{\partial^2}{\partial \zeta^2}\right]\phi_j(x,\zeta) = 0 \; (j = 1,2), \tag{A3}$$

where $\nu_1$ and $\nu_2$ are the positive real part roots of the characteristic equation

$$c_{33}c_{44}\nu^4 + [c_{13}(c_{13} + 2c_{44}) - c_{11}c_{33}]\nu^2 + c_{11}c_{44} = 0. \tag{A4}$$

For the elastic constants of GaN given above, its roots are purely real and have the values $\nu_1 = 1.589$ and $\nu_2 = 0.623$.

The image displacements are expressed through the stress functions as[20]

$$Ru_r^{\rm im}(x,\zeta)=\frac{\partial}{\partial x}(\phi_1+\phi_2),\quad Ru_z^{\rm im}(x,\zeta)=\frac{\partial}{\partial \zeta}(k_1\phi_1+k_2\phi_2), \tag{A5}$$

where the parameters $k_j$ are given by

$$k_j=\frac{\left(c_{11}/\nu_j^2\right)-c_{44}}{c_{13}+c_{44}}\quad (j=1,2). \tag{A6}$$

The image stress components entering the boundary conditions (6) at the side surface have the form

$$\begin{aligned}R^2\sigma_{rr}^{\rm im}(x,\zeta)&=-(c_{11}-c_{12})\frac{1}{x}\frac{\partial}{\partial x}(\phi_1+\phi_2)-c_{44}\frac{\partial^2}{\partial\zeta^2}[(1+k_1)\phi_1+(1+k_2)\phi_2],\\ R^2\sigma_{rz}^{\rm im}(x,\zeta)&=c_{44}\frac{\partial^2}{\partial x\partial\zeta}[(1+k_1)\phi_1+(1+k_2)\phi_2].\end{aligned} \tag{A7}$$

The solution of the corresponding boundary-value problem for the image fields in an infinite elastic cylinder with a one-dimensional distribution of the intrinsic strains described by a shape function $g(z)$ is the following. The stress functions are

$$\begin{aligned}\phi_1(x,\zeta)&=-\frac{R^2\sigma^0}{c_{44}}\frac{\nu_1}{1+k_1}\int_0^\infty\frac{I_0(qx/\nu_1)}{I_1(q/\nu_1)}\frac{g(q)}{qD(q)}\cos q\zeta\,dq,\\ \phi_2(x,\zeta)&=\frac{R^2\sigma^0}{c_{44}}\frac{\nu_2}{1+k_2}\int_0^\infty\frac{I_0(qx/\nu_2)}{I_1(q/\nu_2)}\frac{g(q)}{qD(q)}\cos q\zeta\,dq.\end{aligned} \tag{A8}$$

The image displacements obtained from Eq. (A8) are given in Eqs. (14) and (15). The corresponding elastic strains can be calculated using the relations

$$e_{rr}^{\rm im}=\frac{\partial u_r^{\rm im}}{\partial r},\quad e_{\theta\theta}^{\rm im}=\frac{u_r^{\rm im}}{r},\quad e_{zz}^{\rm im}=\frac{\partial u_z^{\rm im}}{\partial z},\quad e_{rz}^{\rm im}=\frac{1}{2}\left(\frac{\partial u_r^{\rm im}}{\partial z}+\frac{\partial u_z^{\rm im}}{\partial r}\right). \tag{A9}$$

The explicit expressions for the strain components are

$$e_{rr}^{\rm im}(x,\zeta)=-\frac{\sigma^0}{c_{44}}\int_0^\infty\left[\frac{1}{1+k_1}\frac{I_0(qx/\nu_1)-\frac{I_1(qx/\nu_1)}{(qx/\nu_1)}}{\nu_1 I_1(q/\nu_1)}-\frac{1}{1+k_2}\frac{I_0(qx/\nu_2)-\frac{I_1(qx/\nu_2)}{(qx/\nu_2)}}{\nu_2 I_1(q/\nu_2)}\right]\frac{g(q)}{D(q)}q\cos q\zeta\,dq, \tag{A10}$$

$$e_{zz}^{\rm im}(x,\zeta)=\frac{\sigma^0}{c_{44}}\int_0^\infty\left[\frac{k_1\nu_1}{1+k_1}\frac{I_0(qx/\nu_1)}{I_1(q/\nu_1)}-\frac{k_2\nu_2}{1+k_2}\frac{I_0(qx/\nu_2)}{I_1(q/\nu_2)}\right]\frac{g(q)}{D(q)}q\cos q\zeta\,dq, \tag{A11}$$

$$e_{\theta\theta}^{\rm im}(x,\zeta)=-\frac{\sigma^0}{c_{44}x}\int_0^\infty\left[\frac{1}{1+k_1}\frac{I_1(qx/\nu_1)}{I_1(q/\nu_1)}-\frac{1}{1+k_2}\frac{I_1(qx/\nu_2)}{I_1(q/\nu_2)}\right]\frac{g(q)}{D(q)}\cos q\zeta\,dq, \tag{A12}$$

$$e_{rz}^{\rm im}(x,\zeta)=\frac{\sigma^0}{2c_{44}}\int_0^\infty\left[\frac{I_1(qx/\nu_1)}{I_1(q/\nu_1)}-\frac{I_1(qx/\nu_2)}{I_1(q/\nu_2)}\right]\frac{g(q)}{D(q)}q\sin q\zeta\,dq. \tag{A13}$$


[1] E. Ertekin, P. A. Greaney, D. C. Chrzan, and T. D. Sands, J. Appl. Phys. **97**, 114325 (2005).
[2] F. Glas, Phys. Rev. B **74**, 121302 (2006).
[3] H. Ye, P. Lu, Z. Yu, Y. Song, D. Wang, and S. Wang, Nano Lett. **9**, 1921 (2009).
[4] A. A. Darhuber, T. Grill, J. Stangl, G. Bauer, D. J. Lockwood, J.-P. Noël, P. D. Wang, and C. M. Sotomayor Torres, Phys. Rev. B **58**, 4825 (1998).
[5] S. Keller, C. Schaake, N. A. Fichtenbaum, C. J. Neufeld, Y. Wu, K. McGroddy, A. David, S. P. DenBaars, C. Weisbuch, J. S. Speck, and U. K. Mishra , J. Appl. Phys. **100**, 054314 (2006).
[6] M. Hanke, C. Eisenschmidt, P. Werner, N. D. Zakharov, F. Syrowatka, F. Heyroth, P. Schäfer, and O. Konovalov, Phys. Rev. B **75**, 161303 (2007).
[7] J. Eymery, F. Rieutord, V. Favre-Nicolin, O. Robach, Y.-M. Niquet, L. Fröberg, T. Mårtensson, and L. Samuelson, Nano Lett. **7**, 2596 (2007).
[8] C. Bougerol, R. Songmuang, D. Camacho, Y. M. Niquet, R. Mata, A. Cros, and B. Daudin, Nanotechnology **20**, 295706 (2009).
[9] O. Landré, D. Camacho, C. Bougerol, Y. M. Niquet, V. Favre-Nicolin, G. Renaud, H. Renevier, and B. Daudin, Phys. Rev. B **81**, 153306 (2010).
[10] V. M. Kaganer, M. Wölz, O. Brandt, L. Geelhaar, and H. Riechert, Phys. Rev. B **83**, 245321 (2011).
[11] M. Wölz, V. M. Kaganer, O. Brandt, L. Geelhaar, and H. Riechert, Appl. Phys. Lett. **98**, 261907 (2011).
[12] M. V. Barton, J. Appl. Mech. **8**, 97 (1941).

[13]S. Timoshenko and J. N. Goodier, *Theory of Elasticity* (McGraw-Hill, New York, 1951).
[14]H. S. Levine and J. M. Klosner, ASCE J. Eng. Mech. **93**, 157 (1967).
[15]Z. Zhong and Q. P. Sun, Int. J. Solids Struct. **39**, 5753 (2002).
[16]D. K. Bowen and B. K. Tanner, *High Resolution X-Ray Diffractometry and Topography* (Taylor & Francis, London, 1998).
[17]P. F. Fewster, *X-Ray Scattering from Semiconductors* (Imperial College Press, London, 2000).
[18]U. Pietsch, V. Holý, and T. Baumbach, *High-Resolution X-Ray Scattering: From Thin Films to Lateral Nanostructures* (Springer, Berlin, 2004).
[19]M. Birkholz, *Thin Film Analysis by X-Ray Scattering* (Wiley, Weinheim, 2006).
[20]H. A. Elliott, Proc. Cambridge Philos. Soc. **45**, 621 (1949).
[21]A. Yu. Belov, in *Elastic Strain Fields and Dislocation Mobility*, edited by V. L. Indenbom and J. Lothe (North-Holland, Amsterdam, 1992), Chap. 6, p. 391.
[22]V. L. Indenbom, in *Elastic Strain Fields and Dislocation Mobility* (Ref. 21), Chap. 1, p. 1.
[23]A. Polian, M. Grimsditch, and I. Grzegory, J. Appl. Phys. **79**, 3343 (1996).